JPE 15-5-17

http://dx.doi.org/10.6113/JPE.2015.15.5.1305
ISSN(Print): 1598-2092 / ISSN(Online): 2093-4718

A Magnetic Energy Recovery Switch Based Terminal Voltage Regulator for the Three-Phase Self-Excited Induction Generators in Renewable Energy Systems

Yewen Wei*, Longyun Kang†, Zhizhen Huang*, Zhen Li*, and Miao miao Cheng**

*,†New Energy Research Center, Electric Power College, South China University of Technology, Guangzhou, China
**College of Electrical and Information Engineering, Hunan University, Changsha, China

Abstract

Distributed generation systems (DGSs) have been getting more and more attention in terms of renewable energy use and new generation technologies in the past decades. The self-excited induction generator (SEIG) occupies an important role in the area of energy conversion due to its low cost, robustness and simple control. Unlike synchronous generators, the SEIG has to absorb capacitive reactive power from the outer device aiming to stabilize the terminal voltage at load changes. This paper presents a novel static VAR compensator (SVC) called a magnetic energy recovery switch (MERS) to serve as a voltage controller in SEIG powered DGSs. In addition, many small scale SEIGs, instead of a single large one, are applied and devoted to promote the generation efficiency. To begin with, an expandable mathematic model based on a *d-q* equivalent circuit is created for parallel SEIGs. The control method of the MERS is further improved with the objective of broadening its operating range and restraining current harmonics by parameter optimization. A hybrid control strategy is developed by taking both of the stand-alone and grid-connected modes into consideration. Then simulation and experiments are carried out in the case of single and double SEIG(s) generation. Finally, the measurement results verify that the proposed DGS with SVC-MERS achieves a better stability and higher feasibility. The major advantages of the mentioned variable reactive power supplier, when compared to the STATCOM, include the adoption of a small DC capacitor, line frequency switching, simple control and less loss.

Key words: Continuous reactive power compensator, Magnetic energy recovery switch (MERS), Phase lock loop, Self-excited induction generator (SEIG), SVC

I. INTRODUCTION

With ever-increasing concerns over environmental pollution and energy shortages, the development of renewable energy resources have attracted wide interest due to its advantages of being abundant in nature and nearly pollutant free. Small scale wind turbines and hydro turbines are widely installed in distributed generation system (DGS) for remote or isolated areas without grid coverage. The self-excited induction generator (SEIG) is usually applied in DGSs due to its reduced installation cost, lower maintenance requirements, absence of a power supply for excitation and natural protection against system overcurrent [1]. However, when compared with a synchronous generator, the voltage instability and poor efficiency of a SEIG limit its application a lot. In order to steady the voltage, fixed-capacitors (FCs) and dynamic reactive power compensators (DRPCs) are needed for building no-load voltage and for compensating reactive power when a load is fluctuating. Moreover, a feasible approach for promoting generation efficiency is to keep each SEIG outputting its rated power.

Some DRPCs, like thyristor switched capacitors (TSCs), thyristor controlled reactors (TCRs) and static synchronous

Manuscript received Oct. 6, 2014; accepted May 8, 2015
Recommended for publication by Associate Editor Seung-Ho Song.
†Corresponding Author: lykang@scut.edu.cn
Tel: +86-8-711-1193, Fax: +86-8-711-1193, South China Univ. of Tech.
*New Energy Research Center, Electric Power College, South China University of Technology, China
**College of Electrical and Information Eng., Hunan University, China

compensators (STATCOMs), have already been designed to regulate the terminal voltage of induction generators. In [2] and [3], the TSC and TCR are applied in a SEIG power system and a proportional integral (PI) closed-loop feedback is used to realize reference voltage tracking. These articles provide a valuable method for line frequency control. However, triple sized reactors and big capacitors are employed and unacceptable current harmonics are produced at the same time. The STATCOM, as a popular DRPC, is capable of generating inductive or capacitive reactive power. Even though it has a low current distortion rate and a good dynamic response characteristic, it suffers from high frequency switching and a complicated space vector pulse width modulation (SVPWM) control [4]-[6]. Thyristor controlled series capacitors (TCSC) [7], static synchronous series compensator (SSSC) [8] and unified power flow controller (UPFC) [9] have also succeeded in continuous reactive power regulation or power factor correction (PFC). However, they are actually compounded by TSCs or TCRs or STATCOMs and are unfit for low power applications in view of their installation cost.

In consideration of the SEIG, two kinds of mathematic models have been concluded from a lot of articles published in recent years [10]-[14]. For 3-Φ SEIGs, every phase is simplified as a voltage source, a series resistance and a series inductance, and this is named the RX model [15]. The RX model is convenient for steady state analysis but it cannot reflect the dynamic characteristic and it increases the complicacy of modeling in parallel SEIG systems. By considering the variation of the magnetizing inductance caused by loads perturbations, state space modeling is studied in reference [16]. An open matrix model, which is fit for any number of parallel SEIGs, is presented in [17]. This is devoted to an analysis of the steady state and transient performance. With the application of the synchronous rotating coordinate conversion (SRCC), the active power and reactive power current component are easy to work out.

This paper proposes a hybrid renewable energy DGS, which mainly utilizes small-scale wind and water power generation, employs parallel connected SEIGs for energy transformation and a novel SVC device called a magnetic energy recovery switch (MERS) for voltage regulation. First, an expandable model is set up for *n* parallel SEIGs based on the SRCC. Then, the operating principle is introduced for the MERS. In order to broaden its operating range and to restrain current harmonics, an improved control method is studied by parameter optimization. The control strategy, when the DGS stands alone or is connected to a grid, is developed. Simulations and experiments are carried out to validate the performance of the MERS as a voltage regulator. The obtained experimental results support that the proposed DGS with a SVC-MERS has better stability and a higher feasibility.

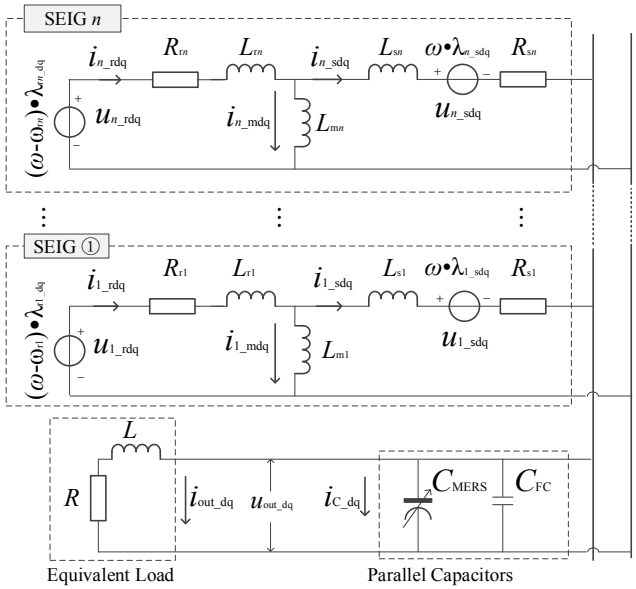

Fig. 1. D-q axis equivalent circuit of the proposed parallel SEIGs using MERS to regulate terminal voltage

TABLE I
VARIABLE DESCRIPTION FOR SEIG

R_{sj}, L_{sj}	Resistance and leakage inductance of stator
R_{rj}, L_{rj}	Resistance and leakage inductance of rotor
L_{mj}	Stator equivalent magnetic inductance
i_{j_sdq}, i_{j_rdq}	Current of stator and rotor
u_{j_sdq}, u_{j_rdq}	Voltage of stator and rotor
i_{j_mdq}	Stator equivalent magnetic current
ω	Angular frequency of rotating magnetic field
ω_{rj}	Angular frequency of the rotor
λ_{j_sdq}, λ_{j_rdq}	Stator fluxes and rotor fluxes.

II. MATHEMATIC MODEL OF PARALLEL SEIGS

Since the integration of many small-scale SEIGs is more flexible and efficient under load changes, *n* different SEIGs are applied here and the *d-q* equivalent circuit of the proposed DGS is shown in Fig. 1. The MERS, denoted by C_{MERS}, works as a controllable capacitance. The FC, denoted by C_{FC}, is used to build the terminal voltage when the SEIG is not loaded. The variable load of the DGS is simplified as an inductance (L) and

$$p\begin{bmatrix} i_{1\_dq} \\ i_{2\_dq} \\ \cdots \\ i_{n\_dq} \\ C_{eq.}\bullet u_{out\_dq} \\ i_{out\_dq} \end{bmatrix} = \begin{bmatrix} G_1 & 0 & 0 & 0 & Z_1 & 0 \\ 0 & G_2 & 0 & 0 & Z_2 & 0 \\ 0 & 0 & \cdots & 0 & \cdots & 0 \\ 0 & 0 & 0 & G_n & Z_n & 0 \\ 1 & 1 & \cdots & 1 & 0 & -1 \\ 0 & 0 & \cdots & 0 & 1/L & -R/L \end{bmatrix} \bullet \begin{bmatrix} i_{1\_dq} \\ i_{2\_dq} \\ \cdots \\ i_{n\_dq} \\ u_{out\_dq} \\ i_{out\_dq} \end{bmatrix} + \begin{bmatrix} B_1 & 0 & \cdots & 0 & 0 & 0 \\ 0 & B_2 & \cdots & 0 & 0 & 0 \\ 0 & 0 & \cdots & 0 & 0 & 0 \\ 0 & 0 & \cdots & B_n & 0 & 0 \\ 0 & 0 & \cdots & 0 & 0 & 0 \\ 0 & 0 & \cdots & 0 & 0 & 0 \end{bmatrix} \bullet \begin{bmatrix} u_{1\_dq} \\ u_{2\_dq} \\ \cdots \\ u_{n\_dq} \\ 0 \\ 0 \end{bmatrix} \quad (1)$$

a resistance (R). The parameters are introduced for the SEIG in Table I in which j is the sequence number.

Based on the state space model and the open matrix model which are mentioned above, a kind of state space matrix is proposed to model parallel SEIGs as shown by equation (1). If j can be 1, 2, to n, the matrix of variables are defined as follows:

$$[i_{j\_dq}]=\begin{bmatrix} i_{j\_sdq} & i_{j\_rdq} \end{bmatrix}^T=\begin{bmatrix} i_{j\_sd} & i_{j\_sq} & i_{j\_rd} & i_{j\_rq} \end{bmatrix}^T$$

$$[u_{out\_dq}]=\begin{bmatrix} u_{out\_d} & u_{out\_q} \end{bmatrix}^T \quad [i_{out\_dq}]=\begin{bmatrix} i_{out\_d} & i_{out\_q} \end{bmatrix}^T$$

$$[i_{C\_dq}]=\begin{bmatrix} i_{C\_d} & i_{C\_q} \end{bmatrix}^T \qquad C_{eq.}=C_{MERS}+C_{FC}$$

$$[u_{j\_dq}]=\begin{bmatrix} u_{j\_sdq} & u_{j\_rdq} \end{bmatrix}^T=\begin{bmatrix} u_{j\_sd} & u_{j\_sq} & u_{j\_rd} & u_{j\_rq} \end{bmatrix}^T$$

Coefficient matrixes, such as $[G_j]$, $[Z_j]$ and $[B_j]$, are expressed in Appendix. For each SEIG, the relationship between L_{mj} and I_{mj} can be represented by the following equation:

$$L_{mj}=\sum_{k=1}^{4} a_{jk} I_{mj}^{\ k-1} \tag{2}$$

Where a_{j0}~a_{j4} are constants. However, they are not fixed in different SEIGs. This model is used for simulation in chapter V.

III. MAGNETIC ENERGY RECOVERY SWITCH

In view of current bi-directional control, the full-bridge type MERS is adopted in this paper. Paper [18] points out that the equivalent capacitance can theoretically be regulated from 0 to infinity by changing the firing angle. It has been employed to correct the power factor or to stabilize terminal voltage of the inductions generator [19]-[22]. However, some shortcomings have gradually emerged such as an incomplete mathematical model, unacceptable harmonics, hard to realize accuracy control and a limited operating range. This section aims to rebuild the mathematic model and to broaden the regulating range.

A. Principle and Mathematic Model

A schematic of the single phase MERS is shown on the left-top corner of Fig. 2. It consists of four insulated-gate bipolar transistors (IGBTs) (G_1~G_4), a small DC capacitor (C_{dc}) and a reactor ($L_{lim.}$). In order to prevent the capacitor from being shorted, no more than two IGBTs can be opened at the same time. With the phase delay control, the parallel MERS works as a controllable capacitor and its equivalent circuit is also presented below the schematic in Fig. 2. C_{MERS} is the equivalent capacitance. R_{line} is the line resistance. U_L, U_R, U_S and U_{MERS} are the voltage of the power source, load, line resistance and MERS, respectively. I_{MERS} represents the current. The waveforms of U_S, U_{MERS} and I_M are plotted on the right side of Fig. 2 in which the dotted line is the fundamental current.

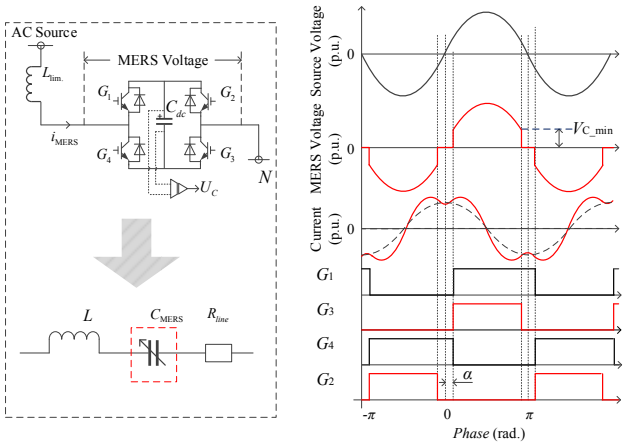

Fig. 2. Schematic and waveforms of single phase MERS.

In reference [19], a MERS is used as a series compensator to regulate the power factor of an AC system and a mathematic model is built by taking the current phase for a reference. In terms of shunt compensation, this model needs to be rebuilt by taking the source voltage phase for a reference instead of the current phase. In addition, the traditional control always gets a high rate of current distortion and overvoltage of the DC capacitor [19]-[22]. These disadvantages lead its regulating range being limited a lot.

Taking the phase of U_S as a reference, G_1 and G_3 are turned on with an alpha (α) delayed. Then, C_{dc} starts to be charged. When V_C is less than $V_{C\text{-}min}$, G_3 is turned off but G_1 is kept open until the U_S phase comes to $\pi+\alpha$. When G_2 and G_4 are turned on, the next half cycle can carry out with a similar process except that the current flow is reversed.

Since its waveform is obviously symmetrical to the vertical axis in Fig. 2, the MERS current can be defined as equation (4) by the fast Fourier transform (FFT).

$$i_{MERS}(\omega t)=\sum_{n=1}^{\infty}\sqrt{2}I_{RMS\_n}\cos(n\omega t),\ n=2N-1,\ N\in N^* \tag{3}$$

Where $I_{RMS\text{-}n}$ is the RMS value of the n^{th} harmonic. $\omega=2\pi f$, f is the system frequency. The MERS voltage is formulated as:

$$u_{MERS}(\theta)=\begin{cases} 0 & \theta\in(-\alpha,\alpha)\cup(\pi-\alpha,\pi)\cup(-\pi,-\pi+\alpha) \\ v(\theta),\theta\in[\alpha,\pi-\alpha] \text{ or } -v(\theta),\theta\in[-\pi+\alpha,-\alpha] \end{cases} \tag{4}$$

$$v(\theta)=V_{C\_min}+\sqrt{2}X_{C_{dc}}\sum_{n=1}^{\infty}\frac{I_{RMS\_n}}{n}[\sin(n\theta)-\sin(n\alpha)]$$

Where $\theta=\omega t$, $X_{Cdc}=1/(\omega C_{dc})$, equation (4) can be unfolded and expressed as equation (5) by using the FFT again.

$$u_{MERS}(\omega t)=\sum_{k=1}^{\infty}b_k\sin k\omega t,\quad k=2N'-1,\ N'\in N^* \tag{5}$$

$$b_k=\frac{4V_{C\_min}\cos k\alpha}{k\pi}+\frac{\sqrt{2}X_{C_{dc}}I_{RMS\_k}}{k^2}\bullet\left[1-\frac{2k\alpha}{\pi}-\frac{\sin(2k\alpha)}{\pi}\right]$$

$$-\frac{2\sqrt{2}X_{C_{dc}}}{\pi}\sum_{n=1}^{\infty}I_{RMS\_n}\left[\frac{1}{n+k}\sin(n+k)\alpha+\frac{1}{n-k}\sin(n-k)\alpha\right]$$

In addition, the RMS value of the fundamental voltage can be described as:

$$U_{RMS\_1}=U_{V_{C\_min}}+U_\alpha-U_x \tag{6}$$

TABLE II
SINGLE PHASE MERS SPECIFICATIONS

Phase rated voltage, U_s	380 V
AC source frequency, f	50 Hz
Current -limiting reactor, L	33.77 mH
Small dc-capacitor, C	60 uF
Line equivalent resistance, R_{line}	0.1 Ω

$$U_{V_{C\_min}} = 2\sqrt{2}V_{C\_min}\cos\alpha/\pi$$

$$U_\alpha = [\pi - 2\alpha - \sin(2\alpha)]I_{RMS\_1}\bullet X_{C_{dc}}/\pi$$

$$U_x = \frac{4\cos\alpha}{\pi}\sum_{n=3}^{\infty}\frac{I_{RMS\_n}}{(n-1)}\sin(n\alpha) - \frac{4}{\pi}\sum_{n=3}^{\infty}\frac{I_{RMS\_n}}{(n+1)(n-1)}\sin(n+1)\alpha$$

Finally, the equivalent capacitive reactance is obtained as:

$$X_{MERS} = U_{RMS\_1}/I_{RMS\_1} = X_{V_{C\_min}} + X_\alpha - X_x \quad (7)$$

$$X_{V_{C\_min}} = 2\sqrt{2}V_{C\_min}\cos\alpha/(\pi I_{RMS\_1})$$

$$X_\alpha = [1 - 2\alpha/\pi - \sin 2\alpha/\pi]\bullet X_C$$

$$X_x = \frac{4}{\pi I_{RMS\_1}}\sum_{i=3}^{\infty}\left[\frac{I_{RMS\_i}}{(i-1)}\sin(i\alpha)\bullet\cos\alpha - \frac{I_{RMS\_i}}{(i+1)(i-1)}\sin(i+1)\alpha\right]$$

B. Variable Reactive Power Characteristic

In view of the negligible line resistance, the reactive power of the MERS branch is denoted by:

$$Q_{out} = \omega C_{dc}E^2/(k_x - k_0) = Q_0 \bullet F(\alpha, V_{C\_min}) \quad (8)$$

Where E is the RMS value of the source voltage, $X_{MERS} = k_x \cdot X_C$ and $X_L = k_0 \cdot X_C$, k_0 is a constant, and k_x is a variable decided by α and $V_{C\text{-}min}$ as deduced in equation (7). F is defined as a function with double variables, $Q_0 = \omega CE^2$.

The complexity of X_{MERS} brings great difficulty in terms of ascertaining the function F. To study the characteristic of the output reactive power, a single phase MERS has been modeled in PSIM with the parameters shown in Table II.

An array of simulation results, by means of regulating α and $V_{C\text{-}min}$ continuously and separately, has been measured. It has been traced out to compare with the theoretical curves obtained from equation (7) and (8) a shown in Fig. 3. The features of Q_{out} between α and $V_{C\text{-}min}$ include: (i) While $V_{C\text{-}min}$ is equal to zero, Q_{out} keeps growing exponentially with a rising α. (ii) While α is fixed as a constant, Q_{out} decreases linearly as $V_{C\text{-}min}$ increases. With the utilization of the linear fitting method, the proposed function F can be described as:

$$F(\alpha, V_{C\_min}) = K_\alpha e^{T_x\bullet\alpha} - K_V \bullet V_{C\_min} \quad (9)$$

In which K_α, T_x and K_V can be figured out by using the least square method (LSM).

C. Control Parameters Optimization

Although the scope of the variable capacitance is theoretically unlimited, it only operates in a small range on account of the unavoidable ascending current harmonics in practical applications. Nevertheless, optimizing the selection of the control parameters may make it possible to reduce the production of current harmonics and it is a unique method for

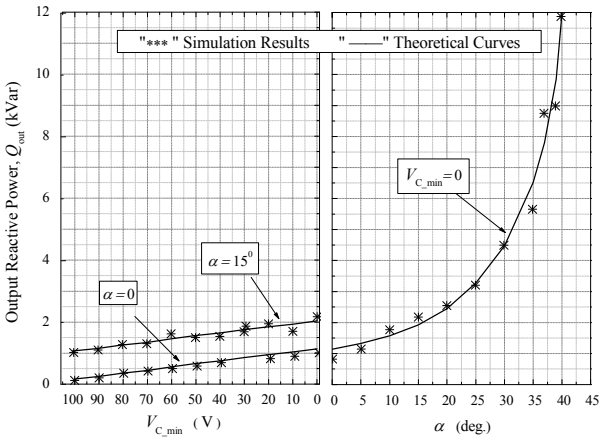

Fig. 3. Equivalent capacitance feature of single phase MERS.

widening the adjusting range of a MERS to some extent. Another challenge when charging current, is the voltage of the DC capacitor which becomes too high. This is caused by the increasing to withstand itself and the IGBTs. Moreover, the current limiting reactor has a significant impact on the current quality and compensation range of the capacitive reactive power. Two solutions, regarding all of these problems, have already been enforced and they have achieved a distinct effect in terms of improving the performance of a MERS. They are introduced in detail below:

1) Make the Match of the Control Parameters - (α, $V_{C\text{-}min}$): In reference [21] and [22], the expected Q_{out} is carried out through altering α or $V_{C\text{-}min}$ asynchronously. This implies that $V_{C\text{-}min}$ is forced to zero when α is adjustable and vice versa. This simple manner has disadvantages such as: (i) it is not possible to restrain current harmonics once the aim of Q_{out} is ascertained. (ii) The maximum α, as well as the largest Q_{out}, is mainly confined due to the finite ability of capacitive pressure. (iii) The growth rate of the current total harmonic distortion (THD) appears too fast to be accepted as introduced in reference [15].

In consideration of the rebuilt MERS voltage equation (6), the combination control method upon α and $V_{C\text{-}min}$ is probably effective in perfecting the system performance. Due to an increase of α or $V_{C\text{-}min}$, which leads to an entirely opposite effect on the reactive power production, there are at least two ways to get the expected Q_{out}. In other words, any Q_{out} can be acquired either by regulating $V_{C\text{-}min}$, by adjusting α, or by changing them both at the same time. There are many operating points on the equivalent power line (EPL) which get the same reactive power. Thus, one can be selected to suppress current harmonic or to avoid DC-capacitor overvoltage or breakdown. To realize the same reactive power output, two points on an EPL (5.31kVar) are applied and the characteristics via comparing the MERS voltage and current have been displayed in Fig. 4. The MERS peak voltage of point (25^0, 0V) is higher than that of point (28^0, 58V). The amplitude of the right side current appears lower than that of the left current. However, the triple harmonic is apparently reduced at point

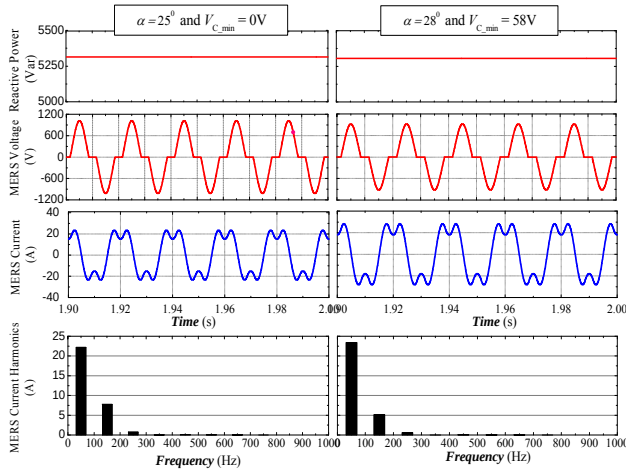

Fig. 4. Comparison of MERS peak voltage and current harmonics at different operation points.

$V_{C\text{-min}} \neq 0$. This proves that there really exists an optimum point, by combining α and $V_{C\text{-min}}$, on an EPL to meet the special requirements for improving MERS performance.

2) Choose a Suitable Reactor: Generally speaking, a reactor is devoted to slow down the growth of the charging/discharging current for a parallel MERS. A large inductive reactance would neutralize the emitted capacitive reactive power which will in turn narrow the compensation range. Therefore, the proportionality coefficient k_0 mentioned in equation (8) should be prudently selected.

Table III, in which the 3rd harmonic is excluded from the current, reflects the relationship between k_0, THD_i and Q_{out} by simulation. Both the THD_i and Q_{out} gradually decline at any of the same working points when k_0 keeps ascending. Regardless of how the reactor changes, the THD_i increases alone with α or $V_{C\text{-min}}$ becomes larger and larger. In conclusion, the coefficient k_0 is determined by the maximum THD of the MERS current. Based on the above analysis, multiple purposes ought to be satisfied for the control parameters optimization and are stated as follows:

$$\begin{cases} EPL: V_{C\_min} = \dfrac{K_\alpha}{K_V} e^{T_s \cdot \alpha} - \dfrac{Q_{(\alpha, V_{C\_min})}}{K_V \bullet Q_0} \\ Q_{(\alpha, V_{C\_min})} \in [Q_{min}, Q_{max}]\big|_{k_0} \\ V_{C\_peak}\big|_{(\alpha, V_{C\_min})} < V_{C\_max} \\ THD_i\big|_{(\alpha, V_{C\_min})} < THD_{max} \end{cases} \quad (10)$$

Where $Q_{(\alpha,\ Vc\text{-min})}$ means the generated reactive power at any working point. The first formula is elicited from equation (9). The third formula limits any dc capacitor voltage not above $V_{C\text{-max}}$. The last one implies that current distortion rate must be lower than the acceptable THD_{max}.

3) Search for the Most Suitable α and $V_{C\text{-min}}$: With the application of synchronous control, response speed of a MERS as a DRPC is hard to accelerate unless the precision of every controlling cycle is enhanced. In view of the α changed in discrete from, the output reactive power must be discontinuous.

TABLE III
CHARACTERISTICS OF DIFFERENT REACTORS EMPLOYED

k_0	(kVar) or (%)	α=0, $V_{C\text{-min}}\neq 0$		$V_{C\text{-min}}$=0, $\alpha \neq 0$			
		100V	50V	5^0	15^0	25^0	35^0
0.35	Q_{out}	1.06	1.01	1.44	2.58	3.37	4.23
	THD_i	9.4	3.64	1.31	2.80	2.99	4.68
0.25	Q_{out}	1.58	1.85	2.30	2.91	3.87	5.45
	THD_i	11.46	3.87	2.03	3.81	3.00	1.40
0.20	Q_{out}	2.23	2.52	3.09	3.67	5.31	6.73
	THD_i	6.34	3.59	2.67	4.50	4.73	3.94
0.15	Q_{out}	4.72	5.40	6.67	7.86	9.22	11.8
	THD_i	9.07	3.71	3.20	4.84	8.57	11.7

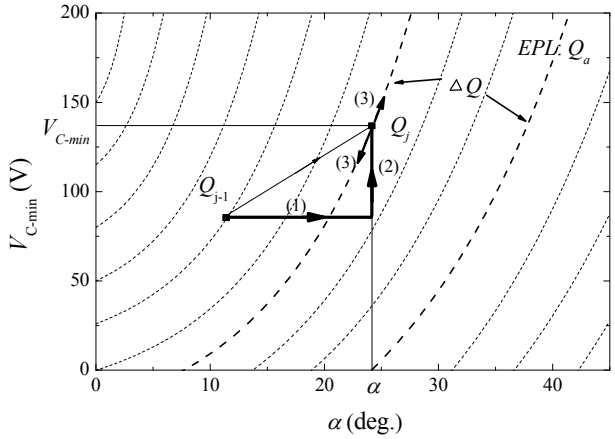

Fig. 5. Approach applied to search the most suitable EPL point

Therefore, the expected Q_{out} can be divided into two parts as follows:

$$Q_{out} = Q_\alpha + \Delta Q = Q_{out}\big|_{(\alpha, 0)} + \Delta Q \quad (11)$$

Where Q_α is generated by α. ΔQ is an error adjusted by $V_{C\text{-min}}$.

Actually, α and $V_{C\text{-min}}$ are complementary in terms of producing continuous reactive power as shown in Fig. 5. The dotted line is a cluster of EPL. In the process of the reactive power changed from $Q_{j\text{-}1}$ to Q_j, α is first increased to reach the EPL Q_α, and then $V_{C\text{-min}}$ is regulated to reach the target value, Q_{out}. The third step is searching for the most suitable point based on equation (9). In Fig. 5, the bold solid lines mean the practical searching path for obtaining the most suitable working point. The special $V_{C\text{-min}}$ can be calculated by V_0+$K\Delta Q$, in which V_0 and K are constants which are worked out by the linear fitting method (LFM).

4) Improved Performance as a Shunt DRPC: With the proposed parameters optimization control, a lot of working points for the MERS are increased. When compared to reference [21], every Q_{out} corresponds to an EPL line but not a single point. Furthermore, the regulating range of X_{MERS} is broadened and satisfies the conditions of the THD_i and $V_{C\text{-peak}}$ limitations of grid. The curves, as measured by simulation, reveal the effect as shown in Fig. 6(a) and Fig. 6(b). The dotted lines, with the application of the control method mentioned in reference [21], are measured for comparison. When the THD_i is lower than 6.0% and $V_{C\text{-peak}}$ does not exceed double V_{C0}, the

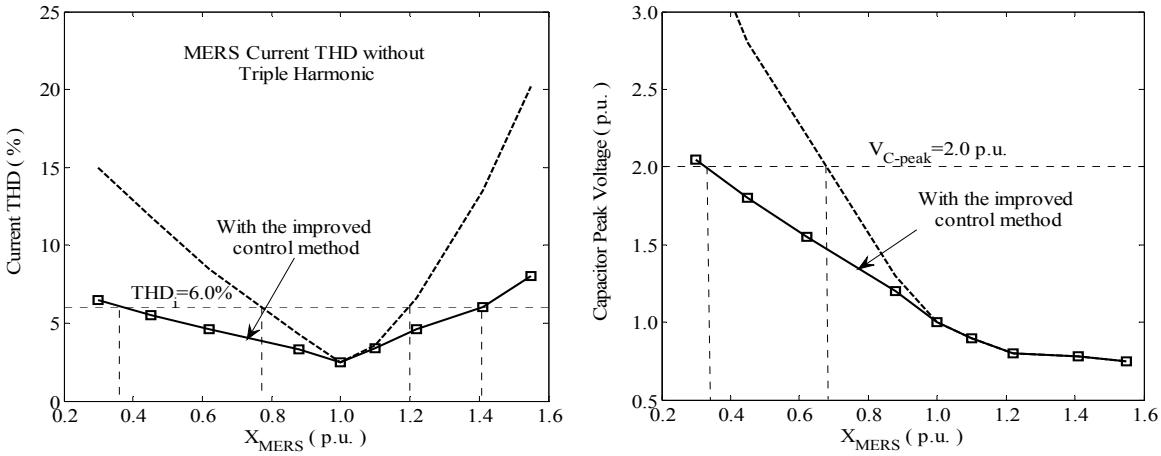

(a) Current THD without triple harmonic. (b) Capacitor peak voltage.

Fig. 6. Comparison of regulating range of X_{MERS}.

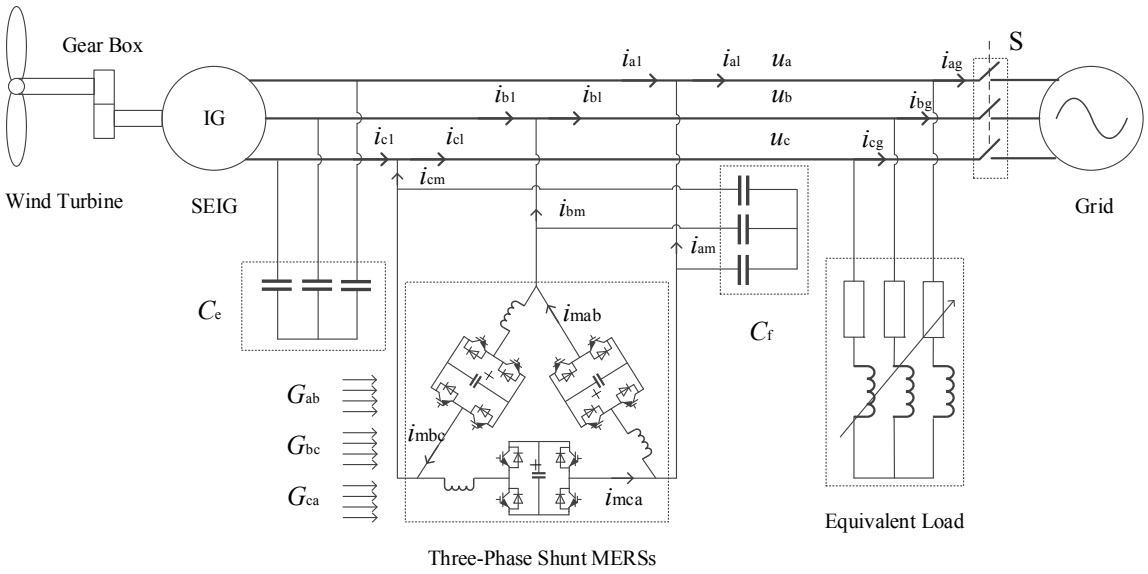

Fig. 7. Schematic of SEIG-based power system using a three phase MERSs as a voltage or reactive power regulator.

maximum X_{MERS} rises from 1.2 p.u to 1.4 p.u, and the minimum X_{MERS} declines from 0.7 p.u to 0.35 p.u. V_{C0} is the capacitor peak voltage of the working point (0^0, 0V).

D. Development of Three-Phase MERSs

For a 3-Φ system, three MERSs are used, as shown in Fig. 7, and connected in delta formation for eliminating the triple current harmonics. The load is equivalent to a changeable resistance and inductance. Power can also flow into the AC grid by operating switch 'S' in case it is needed. Each MERS is controlled independently and IGBTs in the same position but in different MERSs are switched by three-phase symmetrical signals. Therefore, only four control signals needs to be supplied even though double the number of switches is used when compared to STATCOMs. In addition, the MERS works in the line frequency and generates less switching loss. With the help of FCs, the 3-Φ MERSs can supply a large range of reactive power for SEIG power systems. A kind of multiple SEIGs power system is going to be studied and tested by simulation and experiments in section V.

IV. SYSTEM CONTROL

In order to achieve voltage phase detection and magnitude measurement, the phase lock loop (PLL) technique is studied in this section. Then, a *d-q* model of the three phase delta-connected MERSs is created and a uniform control strategy is proposed for voltage regulation under the state of stand-alone operation and power factor correction in the case of connection to the grid.

A. Phase Lock Loop Technique

Assume that the input three phase voltages are three cosine functions with the same amplitude (U_m), but with phases delayed 120^0 in sequence. Therefore, a new equation is obtained as:

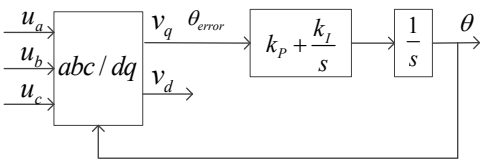

Fig. 8. Schematic of applied closed loop control.

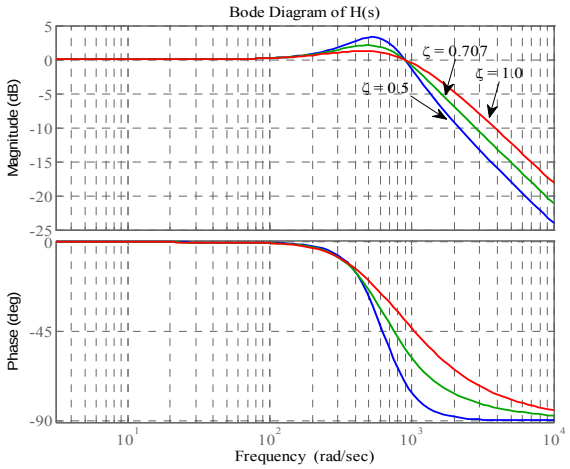

Fig. 9. Bode diagrams of H(s) for different values of ζ.

$$\begin{bmatrix} v_d \\ v_q \end{bmatrix} = \frac{2}{3}\begin{bmatrix} \cos\theta & \cos(\theta-\frac{2\pi}{3}) & \cos(\theta+\frac{2\pi}{3}) \\ \sin\theta & \sin(\theta-\frac{2\pi}{3}) & \sin(\theta+\frac{2\pi}{3}) \end{bmatrix}\bullet\begin{bmatrix} u_a \\ u_b \\ u_c \end{bmatrix} = U_m\bullet\begin{bmatrix} \cos(\theta-\theta^*) \\ \sin(\theta-\theta^*) \end{bmatrix} \quad (12)$$

Where θ is the synchronous phase of the voltage, and θ^* is the actual phase. When the error between θ and θ^* becomes very small, v_d and v_q tend to be U_m and $U_m \cdot (\theta-\theta^*)$, respectively. Therefore, a closed loop control is proposed to gain a precise voltage phase and amplitude as shown in Fig. 8.

The transfer function of this control loop is revealed as $H(s)$. Bode diagrams of $H(s)$ are depicted in Fig. 9 according to different control parameters, k_P and k_I. The performance of ζ=0.707 is more stable and is selected here.

$$H(s) = \frac{sk_P + k_I}{s^2 + sk_P + k_I} = \frac{sk_P/k_I + 1}{s^2/k_I + sk_P/k_I + 1} \quad (13)$$

Where, ζ is defined as follows:

$$\zeta = 0.5k_P/\sqrt{k_I} \quad \text{and} \quad k_I = (200\pi)^2$$

Furthermore, the three phase currents are also assumed to be cosine functions, but with the same magnitude (I_m). The *d-q* current components are described as:

$$\begin{bmatrix} I_d \\ I_q \end{bmatrix} = [G(\theta)]\bullet\begin{bmatrix} i_a \\ i_b \\ i_c \end{bmatrix} = I_m\bullet\begin{bmatrix} \cos\varphi \\ \sin\varphi \end{bmatrix} = \begin{bmatrix} I_{AP} \\ I_{RP} \end{bmatrix} \quad (14)$$

Where I_{AP} and I_{RP} refer to the active power current component and the reactive power current component, respectively.

B. Control Strategy

With the use of the mentioned PLL, the *d-q* model of a 3-Φ delta-connected MERSs can be described as:

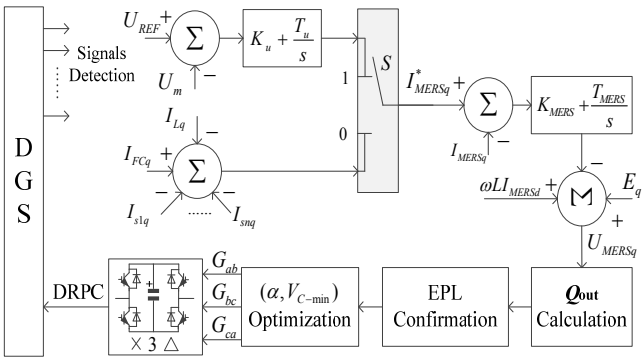

Fig. 10. Schematic of the proposed control strategy.

$$\begin{cases} E_d - U_{MERSd} - \omega LI_{MERSq} = (sL + R_{line})I_{MERSd} \\ E_q - U_{MERSq} + \omega LI_{MERSd} = (sL + R_{line})I_{MERSq} \end{cases} \quad (15)$$

Where E_d, E_q, U_{MERSd}, U_{MERSq}, I_{MERSd} and I_{MERSq} refer to the grid voltage, MERS voltage and MERS current, respectively. Only the lower formula of equation (15) is studied on account of the negligible active power current component.

To realize stability regulation, a negative feedback function is introduced and defined as:

$$U_{MERSq} = -(K_{MERS} + T_{MERS}/s)\bullet(I^*_{MERSq} - I_{MERSq}) + E_q + \omega LI_{MERSd} \quad (16)$$

Where K_{MERS} and T_{MERS} are the proportionality coefficient and the time constant, respectively. The working state of this DGS can be described by a switch function as:

$$S = \begin{cases} 1, & \text{Stand-alone} \\ 0, & \text{Grid-Connected} \end{cases} \quad (17)$$

Then, the reference current (I^*_{MERSq}) can be expressed as:

$$I^*_{MERSq} = S\bullet\frac{K_u\bullet s + T_u}{s}\bullet(U_{REF} - U_m) + (S-1)\bullet(I_{FCq} - \sum_{j=1}^{n} I_{j,sq} - I_{Lq}) \quad (18)$$

Where U_{REF} means the reference phase voltage of the DGS, and I_{FCq}, I_{Lq} and I_{siq} are the reactive power current components of each of these branches. K_u and T_u are the proportionality coefficient and time constant of this voltage control loop. In addition, Q_{out} is obtained on the basis of equations (8) ~ (10) as:

$$Q_{out} = \frac{Q_0}{k_0}\bullet\frac{E - U_{MERSq}}{2U_{MERSq} - E} \quad (19)$$

From equation (8), the primary operating point (α, 0) is ascertained by:

$$\alpha = F^{-1}(Q_\alpha / Q_0) \quad (20)$$

Then, $V_{C\text{-min}}$ can be worked out by equation (9).

The proposed control strategy is shown in Fig. 10. The voltage or current signals are detected from the DGS at first and transformed to *d-q* axis signals using the SRCC. The reference current, I^*_{MERSq}, is determined by two different operating modes. Then, equation (16) and (18) are applied to get the control variable, U_{MERSq}. The expected Q_{out} can be achieved with equation (19) and used for EPL confirmation. Lastly, the control parameters are optimized and the control signals are generated to drive the 3-Φ MERSs to provide DRPC for the DGS.

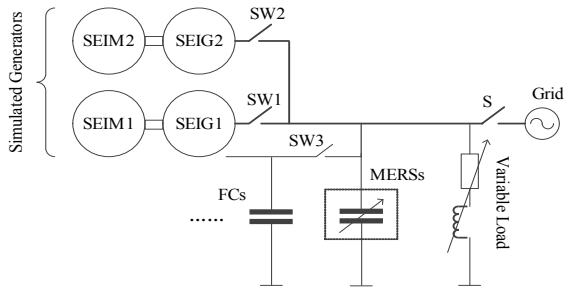

Fig. 11. Diagram of the system construction of experimental DGS.

TABLE IV
SPECIFICATIONS OF THE EXPERIMENTAL DGS

SEIMs Simulated Wind Power System	Rated power	11kW, 4kW
	Rated current	23A, 8.8A
	Rated voltage	380V
	Frequency	50Hz
Three-phase MERSs	DC-capacitors	40*u*F, 1250V
	k_0	0.2
	IGBTs	100A, 1200V
Fixed-capacitors (FCs)	Rated voltage	450V
	Connect- type	Δ
	Capacitance	47.2*u*F, 62.9*u*F, 78.6*u*F
Variable Load	Real power	0 ~ 15 kW
	Reactive power	0 ~ 25 kVar

V. SIMULATION AND EXPERIMENTS VERIFICATION

A small-scale DGS with two SEIGs has been developed as well as an equivalent simulation model based on equation (1) and the same parameters used in PSIM. The 3-*Φ* MERSs and groups of FCs are employed to supply continuous reactive power. First, the proposed control strategy is demonstrated in a developed 3-*Φ* MERSs when it connects to a power grid directly. With the novel DRPC device, the adjustment of the system voltage or reactive power are verified by both the simulation and experiment results when only one SEIG is powered and the double SEIGs are powered, respectively.

A. Experimental System Construction

A principle diagram of the experimental DGS is shown in Fig. 11. A self-excited induction motor (SEIM) is selected to simulate a wind turbine as a prime mover. SW1, SW2, SW3 and S, are used to realize the different running modes.

The system specifications are revealed in Table IV. A photograph of the designed 3-*Φ* MERSs is shown in Fig. 12(a), and Fig. 12(b) shows a simulation of the wind power system. Expert III, which works as a central controller with an integrated DSP (C6713), is applied here. PE-View 9 is a kind of special control soft for Expert III. The testing equipment includes a TPS 2024 (200MHz), a FLUKE 43B POWER QUALITY ANALYZER, etc. In order to achieve practical performance, the parameters of the induction motor are measured and used in the simulation model, as shown in Appendix Table V.

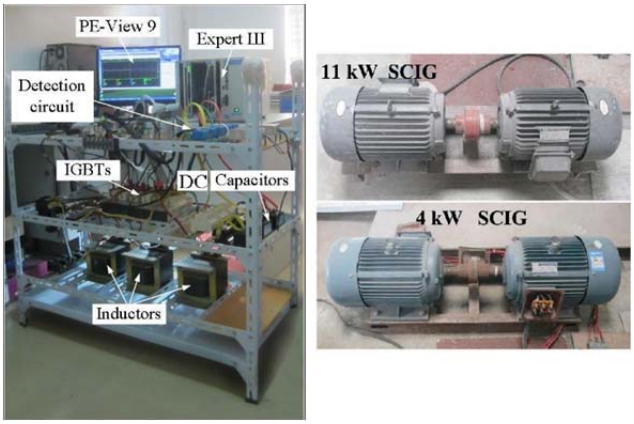

(a) 3-*Φ* MERSs. (b) SEIMs driven SEIGs.

Fig. 12. Photographs of the experimental devices.

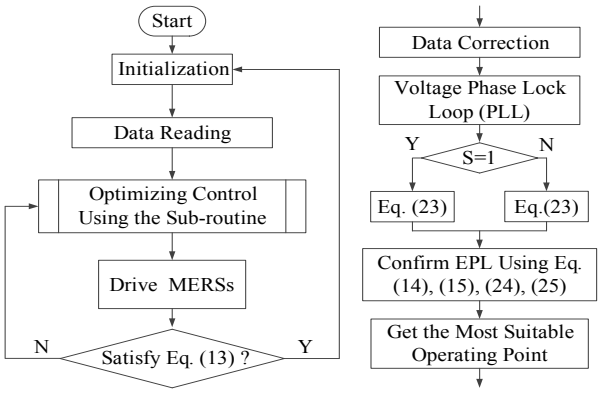

(a) Main program. (b) Sub-routine for optimizing control.

Fig. 13. Schematic of the program running in PE-View 9

B. Verification of the Proposed DRPC

Fig. 13 shows a flow diagram of the applied program. This part only takes the situation of S=0 into account to show that the MERSs can produce a continuously variable reactive power. Some necessary constants are ascertained separately: THD_{max} =6.0%, $V_{C\text{-}peak}$=1000V, Q_0=2.268kvar, ζ=0.707, K_{MERS}=1.15, T_{MERS}=0.0025, and E_q =0. Then, experimental results are obtained as shown in the following pictures.

1) Performance of the Optimized Operating Point: With the parameter optimization control, the MERS current THD and $V_{C\text{-}peak}$ are adjusted by $V_{C\text{-}min}$. Fig. 14 and Fig. 15 reveal the simulation and experimental results, respectively. In Fig. 14(a), both of the two points can generate the same reactive power (EPL=12.45kvar). However, the right figure shows the lower peak-peak MERS voltage and current distortion rates achieved at point (10^0, 15V). Fig. 14(b) demonstrates this feature when the EPL is equal 16.12kvar. Fig. 15(a) and Fig. 15(b) show the experimental results which show that the proposed method is effective.

In addition, different operating points and the

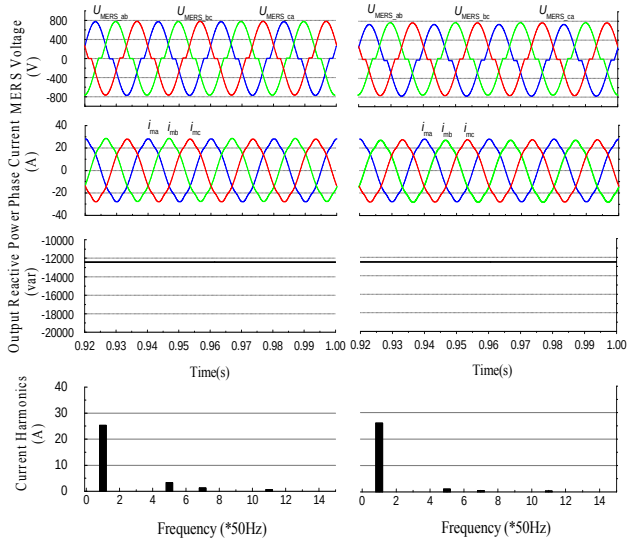

(a) Point (09^0, 0V) & Point (10^0, 15V).

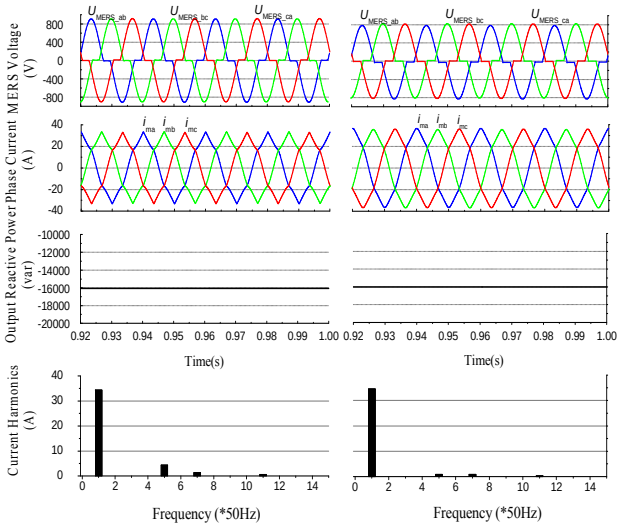

(b) Point (20^0, 10V) & Point (23^0, 43V).

Fig. 14. Simulation of parameters optimization control.

corresponding Q_{out} are applied to calculate some of the coefficients mentioned above using LFM and K_α =1.1, T_x =0.033, K_v =0.002, V_0 =0.00, and K =0.05.

2) Reactive Power Compensation Range Extended: When the conditions of equation (10) are satisfied, the practical range of the reactive power compensation and the operating point are considered and experimented on. Fig. 16(a) shows the THD_i and the capacitor peak voltage when the output reactive power rises and Fig. 16(b) gives its permit working point. The squares connected by solid lines are the experimental results with the proposed parameter optimization control. The squares connected by dotted lines are the experimental results using the control method before improvement. The filled squares reflect the peak voltage of the capacitor and unfilled ones refer to the MERS current THD.

The capacity of the reactive power compensation can be obtained and it can be regulated from 7.5kVar to 22.5kVar

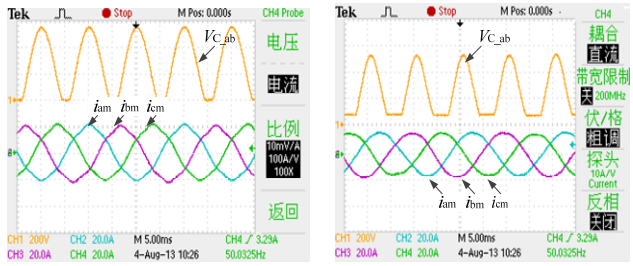

(a) Left Point (09^0, 0V) & Right Point (10^0, 15V).

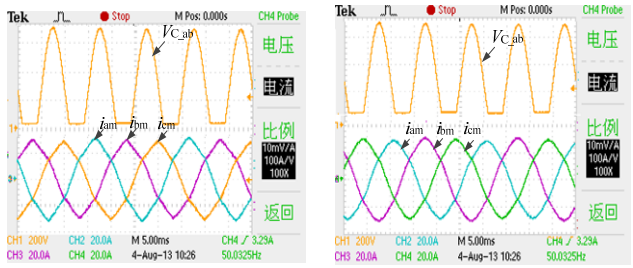

(b) Left Point (20^0, 10V) & Right Point (23^0, 43V).

Fig. 15. Experiment of control parameters optimization.

when the THD_i<6% and the $V_{C\text{-}peak}$<1000V as shown in Fig. 16(a).

In Fig. 16(b), the operating points of the improved MERS are broadened to the large area which is enclosed by four bold lines. In reference [21], the working point is only permitted on the α axis or the $V_{C\text{-}min}$ axis, and the range of the dynamic reactive power is just regulated from 8.0kVar to 16.0kVar. Therefore, both the minimum and maximum Q_{out} are extended in this work.

C. Voltage Regulation for the SEIGs Powered DGS

In this part, the proposed control strategy is verified with the switches S, SW1 and SW3 closed as shown in Fig. 11. The MERSs and the FCs just work as power factor correctors (PFC) for the grid when load is changing. Then, S is open and the voltage of the SEIGs is regulated by the MERSs. Lastly, SW2 is also closed and the experimental results are separately measured when the load goes up or down.

1) Power Factor Correction of the Grid Connected SEIG: When a SEIG connects to a grid, the output voltage is always kept at a rated value since it is fixed by the grid voltage. The most important feature is the transient and steady state performance in terms of power factor correction when the MERSs are applied. With the load increasing or declining, the dynamic and stable characteristics are verified by simulation and experiment studies.

In order to achieve the best performance in terms of power factor regulation, the proportion of K_{MERS} and T_{MERS} needs to keep at 1:1000, which is verified by the simulation. Its effect is shown in Fig. 17(a) and Fig. 17(b) under the conditions of an increasing or decreasing load. Fig. 18(a) and Fig. 18(b) show the dynamic process in the experiments.

By continuously increasing the load, the power factor of the grid is measured and as shown in Fig. 19. The load

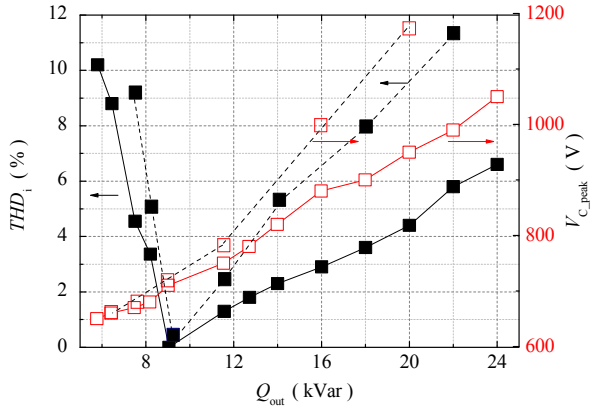

(a) Current distortion rated and peak voltage of DC capacitor.

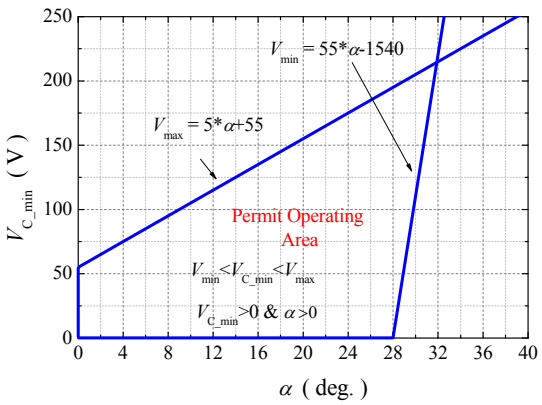

(b) Broadened operating area.

Fig. 16. Steady state characteristics of MERSs.

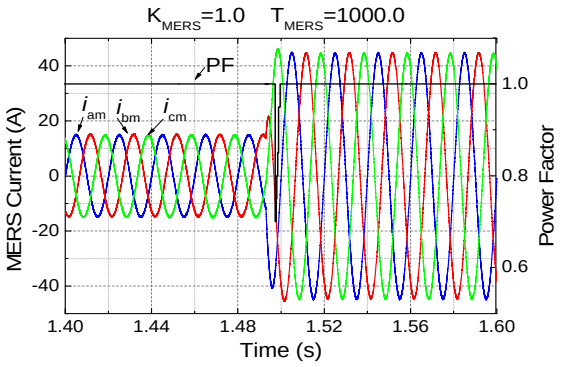

(a) Load increases.

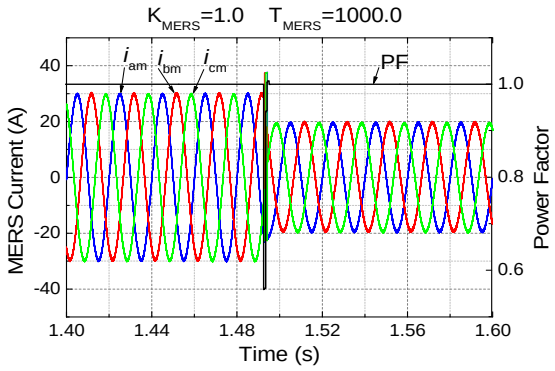

(b) Load decreases.

Fig. 17. Transient characteristics when the proportion between K_{MERS} and T_{MERS} is 0.001.

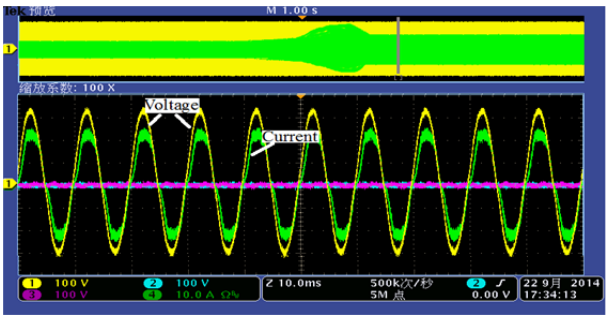

(a) Load increases.

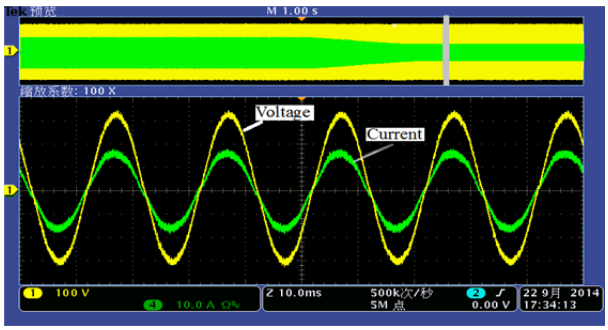

(b) Load decreases.

Fig. 18. Transient characteristic when K_{MERS} =1.22 and T_{MERS} =1350.0 in experiment.

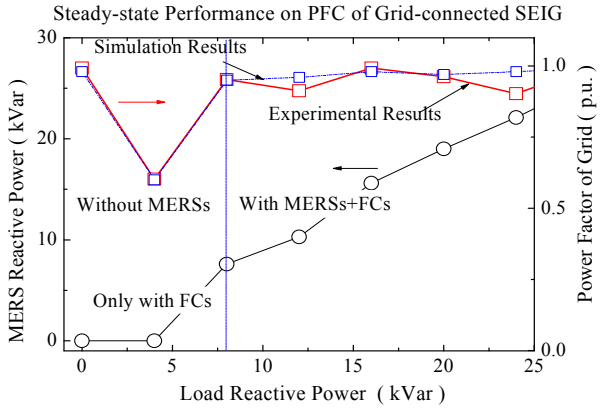

Fig. 19. Steady state performance on power factor regulation.

reactive power is dynamically compensated by the MERSs and FCs as revealed by the solid line of connected circles. The squares connected by solid line or dotted line, show the steady state process of the grid PFC in the simulation and experiment, respectively. Obviously, the power factor can always maintain a unit because the MERSs produce equivalent reactive power to make up for the SEIG leaded by increasing the load. When the output reactive power is lower than 7.5kVar or larger than 22.5kVar, the current THD is measured and shown in Fig. 20(a) and Fig. 20(b).

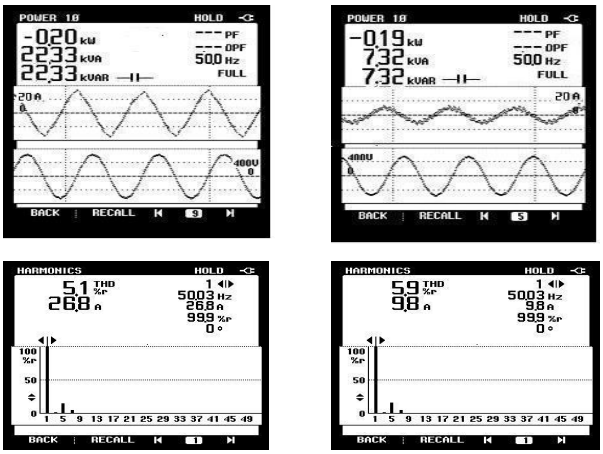

(a) Maximum Q_{out} point. (b) Minimum Q_{out} point.

Fig. 20. Current THD for the boundary operating point.

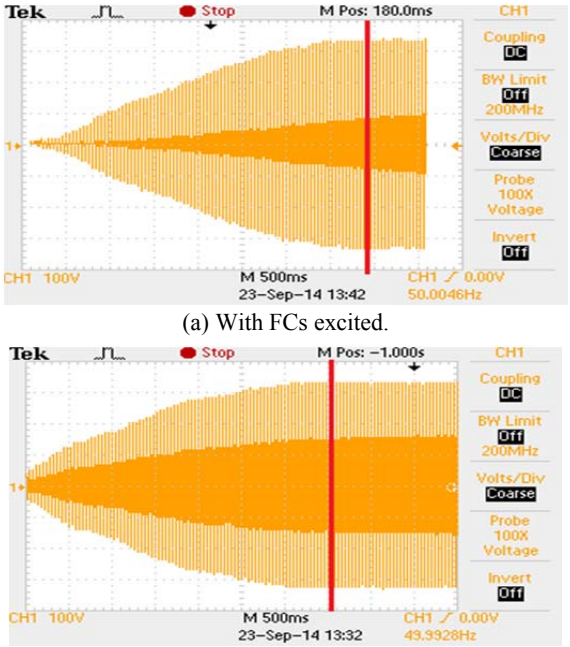

(a) With FCs excited.

(b) With MERSs.

Fig. 21. The process of no-Load voltage building by experiment.

2) Voltage Regulation for a Single SEIG: Fig. 21(a) and Fig. 21(b) show the processes of no-load voltage building with FCs excited and with MERSs. The simulation model shown in Fig. 7 has been built in PSIM. The parameters of this model are the same as those used in the experimental SEIGs as shown in Table V in the Appendix.

The first step is to ascertain a couple of K_U and T_U to get the best transient characteristic. When K_U =1.0 and T_U =1000.0, the simulation results, including the waveforms of three phase voltage, are described in Fig. 22. The bold line means the RMS value of the grid voltage. Then, a group of special K_U and T_U is estimated and used in the experiment on the basis of the simulation results. Fig. 23 shows the experimental results when K_U =3.88 and T_U =3550.0.

3) Voltage Regulation for Double SEIGs: With the parameters

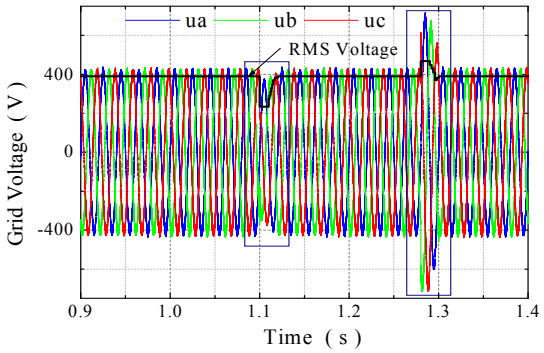

Fig. 22. SEIG's line-line voltage regulation by Simulation.

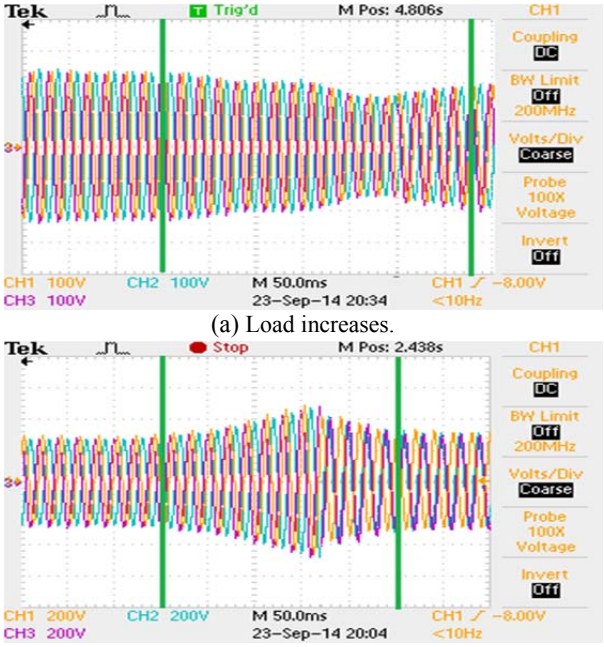

(a) Load increases.

(b) Load decreases.

Fig. 23. Experimental results of SEIG voltage adjusting when K_U =3.88 and T_U =3550.0.

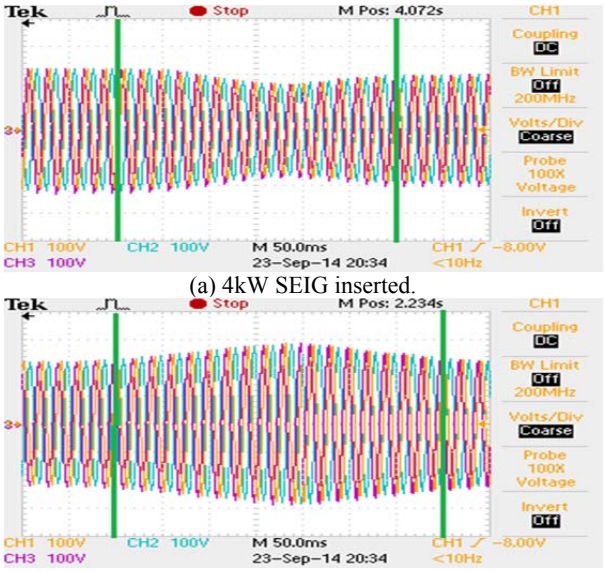

(a) 4kW SEIG inserted.

(b) 4kW SEIG cut off.

Fig. 24. Voltage regulating at the moment of 4kW SEIG inserted in or cut off.

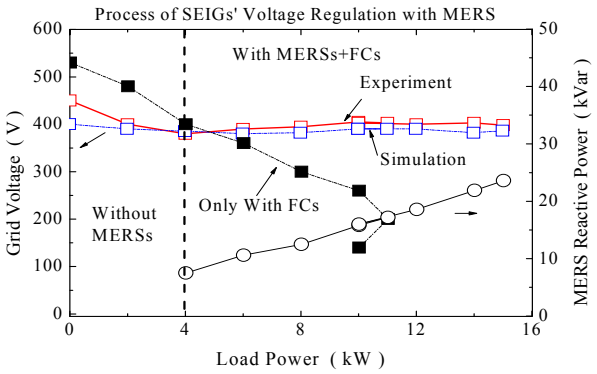

Fig. 25. Stable performance of the developed DGS voltage.

K_U and T_U tested above, the dynamic process of voltage regulation at the moment when a 4 kW SEIG is inserted in or cut off is shown in Fig. 24.

Finally, the voltage regulation of the developed DGS is realized and the curves, as shown in Fig. 25, reflect the characteristic of its steady-state performance. Obviously, the grid voltage is dramatically reduced, as revealed by the dotted line with filled squares, unless the MERSs are installed. The solid line with unfilled circles shows that the output of the MERSs reactive power increases continuously with the rising load power. The unfilled squares which are connected by a solid line and a dotted line, verify that the voltage stability of the DGS can be maintained by the MERSs + FCs. In conclusion, the MERS works as a DRPC in SEIGs powered wind systems and it is verified by both simulation and experimental results.

VI. Conclusion and Future Work

A simple full-bridge MERS which is especially applicable to small-scale DGSs has been studied in this article. A theoretical analysis and experiments are devoted to validate it as a DRPC and to illustrate its feasibility for voltage or reactive power regulation in SEIGs power systems. Both the steady state and transient state experimental results support the conclusion that the MERS is a valuable and reliable reactive power controller. When compared to STATCOMs, the major advantages of the MERS include the adoption of a small DC capacitor, line frequency switching, simple control, and reduced losses. The MERS can also realize reactive power control in micro-grids. This will be investigated at some point in the future.

Appendix

The coefficient matrix mentioned in equation (1) is defined as follows:

$$[G_j]=M_j\bullet\begin{bmatrix} R_{sj}L_{tj} & -\omega_{tj}L_{mj}^2 & -R_{tj}L_{mj} & -\omega_{tj}L_{mj}L_{tj} \\ \omega_{tj}L_{mj}^2 & R_{sj}L_{tj} & \omega_{tj}L_{mj}L_{tj} & -R_{tj}L_{mj} \\ -R_{sj}L_{mj} & \omega_{tj}L_{mj}L_{sj} & R_{tj}L_{sj} & \omega_{tj}L_{tj}L_{sj} \\ -\omega_{tj}L_{mj}L_{sj} & -R_{sj}L_{mj} & -\omega_{tj}L_{tj}L_{sj} & R_{tj}L_{sj} \end{bmatrix} \quad M_j=\frac{1}{L_{mj}^2-L_{sj}L_{tj}}$$

TABLE V
Main Parameters of SEIGs

Parameters	11kW	4kW
Stator resistance (R_s, Ω)	1.0	1.2
Rotor resistance (R_r, Ω)	0.5	0.7
Stator leakage inductance (L_s, *m*H)	5.9	3.7
Rotor leakage inductance (L_r, *m*H)	5.9	3.7
a_{j4}	($\times10^{-6}$)	-6.89	-5.41
a_{j3}	($\times10^{-4}$)	1.38	1.98
a_{j2}	($\times10^{-3}$)	-1.22	-1.52
a_{j1}	($\times10^{-3}$)	1.28	1.33
a_{j0}	($\times10^{-2}$)	4.62	3.66

$$[Z_j]=M_j\bullet\begin{bmatrix} L_{tj} & 0 & -L_{mj} & 0 \\ 0 & L_{tj} & 0 & -L_{mj} \end{bmatrix}^T$$

$$[B_j]=M_j\bullet\begin{bmatrix} -L_{tj} & 0 & L_{mj} & 0 \\ 0 & -L_{tj} & 0 & L_{mj} \\ L_{mj} & 0 & -L_{sj} & 0 \\ 0 & L_{mj} & 0 & -L_{sj} \end{bmatrix}$$

Acknowledgement

This work is supported by Youth Fund of National Natural Science Foundation in China (Grant no.6110418).

References

[1] E. Touti, R. Pusca, J. P. Manata, J. F. Brudny, and A. Chaari, "On the use of a dimmer for a robust frequency control of a self-excited three-phase induction wind generator," *Journal of Power Electronics*, Vol. 14, No. 3, pp. 580-591, May 2014.

[2] T. Ahmed, O. Noro, E. Hiraki, and M. Nakaoka, "Terminal voltage regulation characteristics by static VAR compensator for a three-phase self-excited induction generator," *IEEE Trans. Ind. App.*, Vol. 40, No. 4, pp. 978-988, Aug. 2004.

[3] L. Spasojević, I. Papič, and B. Blažič, "Development of a control algorithm for a static VAR compensator used in industrial networks," *Journal of Power Electronics*, Vol. 14, No. 4, pp. 754-763, Jul. 2014.

[4] B. Singh, S S. Murthy, and S. Gupta, "STATCOM-based voltage regulator for self-excited induction generator feeding nonlinear loads," *IEEE Trans. Ind. App.*, Vol. 53, No. 5, pp. 1437-1452, Oct. 2006.

[5] J.A. Barrado, R. Griñó, and H. Vald-Blavi, "Power-quality improvement of a stand-alone induction generator using a STATCOM with battery energy storage system," *IEEE Trans. Power Del.*, Vol. 25, No. 4, pp. 734-2741, Oct. 2010.

[6] T. Ahmed, K. Nishida, and M. Nakaoka, "A novel stand alone induction generator system for ac and DC power applications," *IEEE Trans. Ind. App.*, Vol. 43, No. 6, pp. 1465-1474, Nov. 2007.

[7] P. K. Tiwari and Y R. Sood, "An efficient approach for optimal allocation and parameters determination of TCSC with investment cost recovery under competitive power

market," *IEEE Trans. Power System*, Vol. 28, No. 3, pp. 2475-2484, Aug. 2013.
[8] M. S. El-Moursi and A. M. Sharaf, "Novel controllers for the 48-pulse VSC STATCOM and SSSC for voltage regulation and reactive power compensation," *IEEE Trans. Power Syst.*, Vol. 20, No. 4, pp. 1985-1997, Nov. 2005.
[9] S. An, J. Condren, and T.W. Gedra, "An ideal transformer UPFC model, OPF first-order sensitivities, and application to scree for optimal UPFC locations," *IEEE Trans. Power System*, Vol. 22, No. 1, pp. 68-75, Feb. 2007.
[10] G. K. Kasal and B. Singh, "Voltage and frequency controllers for an asynchronous generator-based isolated wind energy conversion system," *IEEE Trans. Energy Convers.*, Vol. 26, No. 2, pp. 402-416, Jun. 2011.
[11] S. Kumar and R. Narayan, "Effect of capacitive VAR on performance of three-phase self-excited induction generator," *International Journal of Emerging Technology and Advanced Engineering*, Vol. 12, No. 2, pp. 253-258, Dec. 2012.
[12] R. C. Bansal, "Three-phase self-excited induction generators: An Overview," *IEEE Trans. Energy Convers.*, Vol. 20, No. 2, pp. 292-299, Jun. 2005.
[13] S. Boora, "Analysis of self-excited induction generator under balanced or unbalanced conditions," *International Journal on Electrical and Power Engineering*, Vol. 1, No. 3, pp. 59-63, Dec. 2010.
[14] D. Seyoum, C. Grantham, and M. F. Rahman, "The dynamic characteristics of an isolated self-excited induction generator driven by a wind turbine," *IEEE Trans. Ind. Appl.*, Vol. 39, No.4, pp. 936-944, Jul. 2003.
[15] J. Cidrás and A. E. Feijóo, "A linear dynamic model for asynchronous wind turbines with mechanical fluctuations," *IEEE Trans. Power Syst.*, Vol. 17, No. 3, pp. 681-687, Aug. 2002.
[16] G. S. Kumar and A. Kishore, "Dynamic analysis and control of output voltage of a wind turbine driven isolated induction generator," in *Proc. ICIT*, pp. 494-499, 2006.
[17] F. A. Farret, B. Palle, and M. G. simoes, "State Space Modeling of Parallel Self-Excited Induction Generator for Wind Farm Simulation," in *Proc. IAS*, pp. 2801-2807, 2004.
[18] T. Isobe, J. A. Wiik, T. Kitahara, S. Kato, and K. Inoue, "Control of series compensated induction motor using MERS," in *Proc. PEA&EC*, pp. 1-10, 2007.
[19] J. A. Wiik, O. J. Fonstelien, and R. Shimada, "A MERS type Series FACTS Controller for Low Voltage Ride Through of Induction Generators in Wind Farms," in *Proc. PEA&EC*, pp. 1-10, 2009.
[20] T. Kawaguchi, T. Sakazaki, and T. Isobe, "Offshore wind farm configuration using diode rectifier with MERS in current link topology," *IEEE Trans. Ind. Electron.*, Vol. 60, No. 7, pp. 2930-2937, Jul. 2013.
[21] M. M. Cheng, D. Shiojima, T. Isobe, and R. Shimada, "Voltage control of induction generator powered distributed system using a new reactive power compensator SVC-MERS," in *Proc. PEMCC*, pp. 71-78, 2013.
[22] F. D. Wijaya, T. Isobe, K. Usuki, J. A. Wiik, and R. Shimada, "a new automatic voltage regulator of self-excited induction generator using SVC magnetic energy recovery switch (MERS)," in *Proc. IEPESC*, pp. 697-703, 2008.

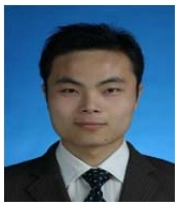

Yewen Wei was born in Hunan province, China. He received his B.S. degree in Measurement and Control Technology for Instrument from Xiangtan University, Xiangtan, China, in 2008. Since 2009, he has been working towards his Ph.D. degree in the School of Electric Power, South China University of Technology, Guangzhou, China. His current research interests include power electronic converters, the application of power electronics in renewable energy systems, reactive power control, harmonics, and power quality compensation systems such as SVC, Magnetic Energy Recovery Switch (MERS), and FACTS devices.

Longyun Kang was born in Jilin, China, in 1961. He received his B.S., degree in Physics from Yanbian University, Yanji, China, in 1982, and his M.S. and Ph.D. degrees in Electrical Engineering from the Department of Engineering, Kyoto University, Kyoto, Japan, in 1996 and 1999, respectively. From 1999 to 2001, he was a Researcher with the Department of Engineering, Tokyo Institute of Technology, Tokyo, Japan. From 2001 to 2006, he was an Associate Professor with the Institute of Mechanical Engineering, Xi'an Jiaotong University, Xi'an, China. Since 2006, he has been with the School of Electric Power, South China University of Technology, Guangzhou, China, where he is presently a Professor, a supervisor of Ph.D. students, and a director of the Guangdong Key Laboratory of Clean Energy Technology. His current research interests include renewable energy and electric vehicles, including wind energy, solar energy conversion, hybrid energy systems and hybrid-drive technology for electric vehicles.

Zhizhen Huang was born in Anhui, China, in 1990. He received his B.S. degree from Xiangtan University, Xiangtan, China, in 2013. Since 2013, he has been working towards his M.S. degree in the School of Electric Power, South China University of Technology, Guangzhou, China. His current research interests include power electronic converters, and MERS based wireless charging technology for vehicles.

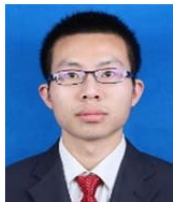

Zhen Li was born in Hunan province, China, in 1992. He received his B.S. degree from the China University of Mining and Technology, Xuzhou, China, in 2014. Since 2014, he has been working towards his M.S. degree in the School of Electrical Power, South China University of Technology, Guangzhou, China. His current research interests include power electronic converters, and power quality compensation systems such as SVC and Magnetic Energy Recovery Switch (MERS).

Miao miao Cheng was born in China, in 1982. She received her M.S. degree from Xi'an Jiaotong University, Xi'an, China, in 2006, and her Ph.D. degree from the Tokyo Institute of Technology, Tokyo, Japan, in 2009, where she worked as a Post-doctor for the following three years. Since 2012, she has been working as an Assistant Professor at Hunan University, Changsha, China. Her current research interests include motor control, energy storage and power electronics.